Rickards, A. M. J., Miles, R. E. H., Davies, J. F., Marshall, F. H., & Reid, J. P. (2013). Measurements of the Sensitivity of Aerosol Hygroscopicity and the kappa Parameter to the O/C Ratio. *Journal of Physical Chemistry A*, *117*(51), 14120-14131. https://doi.org/10.1021/jp407991n

Measurements of the Sensitivity of Aerosol Hygroscopicity and the Kappa Parameter to the O/C Ratio

Andrew M. J. Rickards, Rachael E. H. Miles, James F. Davies, Frances H. Marshall and Jonathan P. Reid*

School of Chemistry, University of Bristol, Bristol, BS8 1TS, UK

ABSTRACT

We report measurements of the subsaturated hygroscopic growth of aerosol particles composed of single organic components of varying oxygen-to-carbon ratio up to relative humidities approaching saturation using the techniques of aerosol optical tweezers and an electrodynamic balance. The variation in the hygroscopicity parameter κ between compounds of even the same O/C ratio is found to be significant with, for example, a range in κ values from 0.12 to 0.38 for compounds with an O/C of 1. The measurements are compared with a review of all of the available literature data for which both the κ value and O/C ratio are reported and a new parameterisation determined. Critical supersaturations predicted using this parameterisation yield values that have associated uncertainties that are comparable to typical uncertainties in experimental measurements of critical supersaturations. However, the systematic variability between κ parameterisations determined from different studies remains large, consistent with the O/C ratio providing only an approximate guide to aerosol hygroscopicity and reflecting significant variations for aerosols of different chemical functionality, composition and oxidation history.

Keywords: Aerosol, single particle, hygroscopicity, organic aerosol, thermodynamics

* Corresponding author: j.p.reid@bristol.ac.uk, tel: +44 117 331 7388

I. INTRODUCTION

Aerosols play an important role in influencing radiative forcing through both the direct effect, where the aerosol particles directly scatter and absorb radiation, and the indirect effect, where the aerosol particles act as cloud condensation nuclei (CCN) and influence cloud droplet number concentrations, size distributions and lifetime.[1–3] Understanding the response of aerosol particle size and composition to changes in relative humidity (RH) is crucial to quantifying their chemical, physical and optical properties and to reducing the large uncertainty in the magnitude of the aerosol indirect effect.[4] An aerosol responds to an increase in relative humidity through the increased partitioning of water into the condensed phase, maintaining equilibrium between the gas and liquid phases. At the microphysical level, an individual aerosol particle grows to a wet diameter $D(RH)$ that is usually referenced to the diameter of the particle under dry conditions, D_0, a ratio referred to as the growth factor, GF (= $D(RH)/D_0$). The dry size reflects the amount of involatile solute associated with the aerosol particle.

Characterising the hygroscopic growth of ambient aerosol has become a routine analytical measurement for accumulation mode particles through the use, for example, of an hygroscopic tandem differential mobility analyser (HTDMA).[5–7] The aerosol sample must be dried before passing it through a first DMA to select a narrow range of particle sizes. The dry aerosol is then humidified under a high RH and passed into a second DMA, which is used to measure the equilibrium size at the elevated RH. In the laboratory, measurements of equilibrium hygroscopic growth on single or multiple component aerosol are performed using ensemble (eg. HTDMA) and single particle techniques (eg. electrodynamic balance and optical tweezers),[8–11] providing controlled studies that can be used to robustly test equilibrium state models and interpret ambient field measurements.

The hygroscopic growth of individual inorganic and organic component aerosol can be rigorously treated with well-established models[12–17] and with approximate treatments derived to capture the phase behaviour.[18,19] One such simplified framework is κ-Köhler theory,[18] a quantitative model describing the degree of hygroscopic growth for an aerosol component by a single hygroscopicity parameter, κ. This parameter can be derived from hygroscopic growth measurements made under subsaturated conditions and can be inferred from the critical supersaturation required to achieve activation of cloud condensation nuclei

(CCN) under supersaturated conditions. For organic species, κ is usually between 0 (non-hygroscopic) and 0.5 (very hygroscopic).[18] Organic components form a substantial proportion of atmospheric aerosol, between 20 and 90 % of the submicron mass depending on region,[20,21] and consists of an enormous variety of different species with a wide range of functional groups for which the hygroscopic properties of only a handful are well characterised.[22,23] Attributing contributions to the hygroscopic growth of ambient aerosol from individual compounds is an intractable approach and the application of a more simplistic model, such as κ-Köhler theory, is unavoidable. A necessary caveat is that more complex models should be applied whenever possible to assess and quantify the level of uncertainty that is acceptable. For example, the change in partitioning of semi-volatile organic components with RH,[24] the occurrence of liquid-liquid phase separation,[25] and the surface tension depression of droplets by surfactants[26] are all examples of thermodynamic properties that still require further detailed investigation.

For subsaturated growth, κ is defined by Petters & Kreidenweis[18] by the parameterisation:

$$GF = \left(1 + \kappa \frac{a_w}{1 - a_w}\right)^{\frac{1}{3}} \quad (1)$$

where a_w is the water activity in the gas phase. This expression is stated in the large particle limit, where the effect of surface curvature can be neglected, and the water activity can be assumed to be equal to the RH. A constant osmotic coefficient must be assumed, an assumption that breaks down as the RH decreases and non-ideality in solute/solvent interactions becomes important. Not only can this framework for quantifying hygroscopicity be used for binary solution aerosol containing a single solute and water, but standard mixing rules such as the Zdanovskii, Stokes, and Robinson (ZSR) assumption can be used to predict the hygroscopicity of mixed component aerosol.[27] To estimate κ from hygroscopic growth measurements it is common practice to make measurements at high RH (0.9 or larger). Petters & Kriedenweis[28] reported that κ values estimated from hygroscopic growth and critical supersaturation measurements agreed to within 30 %, suggesting that the change in κ measured at a water activity, a_w, of 0.9 to the value at the water activity corresponding to activation is small. Although a large number of more recent studies have found consistency (within 10 - 30 %) for the values of κ estimated from subsaturated and supersaturated measurements,[9,18,29–35] larger discrepancies have been found in a significant number of studies.[36–42] The discrepancies have been

attributed to the non-ideal behaviour for supersaturated solutions of solutes,[43,44] the possibility of kinetic limitations on particle drying and the estimation of the dry particle size,[45,46] incorrect assumptions about surface tension effects,[36–42] and the slow dissolution of sparingly soluble compounds.[44,47] However determining the relative importance of these effects may prove difficult as recent research has also shown instrument dependent discrepancies in κ values determined for secondary organic aerosol (SOA).[46,48]

Quantifying the accuracy of any hygroscopicity model for predicting the critical supersaturation for activation of CCN is crucially important for understanding laboratory measurements and the formation of cloud droplets from ambient aerosol.[49] At activation, the water activity in an aerosol particle is typically larger than 0.99 and approaches a value of 1. Indeed, under such limiting conditions it is important that the functional forms chosen to reproduce the hygroscopic response have the correct form to characterise the limiting behaviour;[50] large uncertainties in the water activity at activation can result even from the appropriateness of the parameterisation chosen to represent the relationship between water activity and solute concentration (or mass fraction of solute).

Examples of the variability in the theoretical treatments of hygroscopicity for three typical single organic component aerosol (malonic acid, levoglucosan and adipic acid) are shown in Figure 1, using four well-established models. The Extended Aerosol Inorganics Model (E-AIM) was implemented by Clegg et al. to treat the solution thermodynamics of the H^+-NH_4^+-Na^+-SO_4^{2-}-NO_3^--Cl^--H_2O system.[12,14] It was later extended to include organic components using the widely used UNIversal quasichemical Functional-group Activity Coefficient (UNIFAC) model.[51] In some cases, the parameters for certain functional groups have been modified according to measurements made on single organic aerosol particles using an electrodynamic balance by Peng et al.[13] The Aerosol Diameter Dependent Equilibrium Model (ADDEM) was developed by Topping et al. to describe the thermodynamic behaviour of mixed inorganic salts and is coupled with a diameter dependent Kelvin term to account for surface curvature.[15] The thermodynamic relationships describing water partitioning with varying RH assume the same parametric dependence as E-AIM for inorganic components and UNIFAC for organic components. The Aerosol Inorganic-Organic Mixtures Functional groups Activity Coefficients model (AIOMFAC) is a further group contribution model designed

to determine activity coefficients of chemical species within aerosols containing atmospherically relevant inorganic-organic mixtures and accounts for the interactions of ions and neutral compounds.[16,17]

Although there is considerable variation in the subsaturated growth curves calculated from the models for the three compounds shown in Figure 1, the growth curves are comparable in the dilute solute limit, particularly for the models that are considered to be more reliable (i.e. excluding UNIFAC without the Peng correction). Using equation (1) we can estimate the apparent variation in the value of κ that would be retrieved if these models were used to infer the hygroscopicity parameter at RHs other than at saturation on approach to infinite dilution of the solute; the apparent κ depends strongly on the water activity even at values approaching saturation and varies considerably from system to system. An increase in κ at high RH, as seen in Figure 1, has previously been attributed to the effects of surface activity and non-idealities in the droplets.[26,52] However, in the current simulations the qualitative shape of the dependence of κ on RH reflects deviations from non-ideal behaviour with no accounting for surface tension depression. Even subtle changes in the slope of the growth curve near 100 % RH can significantly alter the value of κ that would be calculated from fitting to equation (1).

In the atmosphere, organic compounds can undergo both functionalisation reactions, notably oxidation to form lower volatility compounds with an increased stoichiometric ratio of oxygen to carbon atoms in a compound (O/C), and fragmentation reactions that lead to higher volatility compounds. The partitioning of semi-volatile and lower volatility organic compounds to the condensed phase leads to the production of SOA. As might be intuitively expected, the hygroscopicity of ambient and chamber SOA, as quantified by the measured value of κ, has been found to correlate with the O/C ratio.[7,20,53] The O/C ratio is conveniently derived from the relative abundance of the ion signal m/z 44 in Aerodyne aerosol mass spectrometry (AMS) measurements of aerosol composition.[20] The m/z 44 signal can be largely attributed to the CO_2^+ ion fragment, and the fraction of the total organic signal due to the m/z 44 ion fragment, f_{44}, has been shown to vary linearly with O/C by the Aiken et al. parameterisation.[7,54]

Our aim here is to examine the relationship between O/C and κ for a range of organic functional groups through a series of new laboratory measurements for organic components of selected O/C ratios. We also provide a comprehensive review of the literature, summarising all previous measurements of κ when the composition of the aerosol, represented by its O/C ratio, has also been reported, spanning the range from around 0 to 2. The literature review encompasses a wide variety of systems spanning field measurements, chamber SOA studies, and single particle laboratory studies, providing data from both natural and synthesised multi-component particles, as well as single component aerosol. Finally, we look at the variability in κ that can be expected for compounds of the same O/C ratio and the implications of this variability for predictions of the critical supersaturation.

II. SINGLE PARTICLE MEASUREMENTS OF SUBSATURATED HYGROSCOPIC GROWTH

We have used two experimental techniques to measure the hygroscopic growth of binary and multi-component aqueous solution droplets containing a range of organic compounds with varying O/C ratio. Using the aerosol optical tweezers technique, we report the equilibrium response in particle size to changes in RH up to a maximum water activity of 0.85. In the second technique, we use an electrodynamic balance to retrieve the hygroscopic growth curve from fast measurements of evaporation kinetics from dilute aqueous solution droplets. This approach allows measurements to be made at water activities as high as >0.99.

II.a Aerosol Optical Tweezers Measurements

Initial measurements of hygroscopic growth using aerosol optical tweezers (AOT) focused on organic aerosol components with O/C=1. A range of species with different functionalities and solubilities were investigated to assess the comparability in their hygroscopic growth and values of κ. Single component aerosol containing organic compounds with a broader range of O/C ratios were then explored, followed by measurements of the hygroscopic properties of droplets containing mixtures of organic compounds. Table 1 summarises the compounds studied.

The aerosol optical tweezers experimental method has been described in detail in our previous publications[55–57] and will only be reviewed briefly here. A single beam gradient force optical trap (optical

tweezers) was formed within a custom built trapping chamber by passing continuous wave laser light at 532 nm through a microscope objective (Olympus oil immersion, × 100). An aqueous solution of each organic compound to be studied was nebulised in to the trapping chamber under a humidified nitrogen flow using an ultrasonic nebuliser (Omron). A single particle was captured from the aerosol plume and trapped at the focal point of the laser beam. Inelastic Raman scattering, Stoke's shifted from the laser wavelength, from chemical species within the droplet was collected by the microscope objective and coupled into a spectrograph (Princeton Instruments). Raman spectra from the trapped droplet were collected every second. An image of the droplet was also recorded using conventional brightfield microscopy. By altering the ratio of wet to dry nitrogen flows, the RH of the environment inside the trapping chamber was varied stepwise between 55 % and 85 %. The trapped droplet was allowed to fully equilibrate after each step change in relative humidity and its hygroscopic response recorded. Accurate measurement of the RH was made using two probes, one before (Vaisala; ± 2 % RH) and one after (Honeywell; ± 2 % RH) the trapping chamber.

The spectroscopic signature from the tweezed aerosol consists of broad spontaneous Stokes bands arising from the Raman excitation of vibrational modes of the molecular constituents of the droplet. Superimposed on this spontaneous scattering background, the Raman intensity is amplified at wavelengths commensurate with whispering gallery modes, providing a unique fingerprint of resonant wavelengths that can be compared with Mie scattering calculations to retrieve both the droplet size and refractive index, both with uncertainties of ±0.05 %.[58,59] A typical variation in droplet size and refractive index with changing RH profile is shown in Figure 2 for hygroscopicity measurements on an aqueous sucrose droplet. The figure shows a clear decrease in size and increase in refractive index as the RH is decreased and water evaporates from the droplet.

To convert the droplet radial data into a *GF* it is necessary to know the solute dry diameter, D_0. This was determined from the volume fraction of organic in the droplet, $V_{f,org}$, estimated from the retrieved refractive index and the total droplet volume, as given by the droplet diameter. Assuming the refractive index of the aqueous organic droplet at a particular RH, RI_{drop}, is the linear sum of the refractive indices of the pure organic component, RI_{org}, and water, RI_w, weighted by their volume fractions present within the droplet, $V_{f,org}$ can be calculated using:

$$RI_{drop} = RI_{org}V_{f,org} + RI_{w}V_{f,w} \quad (2)$$

where $V_{f,w}$ is the volume fraction of water in the droplet (1-$V_{f,org}$) and RI_{drop} is determined from the Raman spectra at each RH. The pure refractive indices for the organic compounds of interest were obtained by measuring the refractive index of a series of aqueous solutions of the organic with increasing mass fraction of solute (mfs) using a refractometer (MISCO Palm Abbe). Solutions were made up to the bulk solubility limit for each compound. From a quadratic fit, the refractive index was estimated at an extrapolated mfs = 1 to determine RI_{org} (Figure 3). Where possible, values determined by this approach were compared with literature values. An estimate of the typical level of uncertainty associated with such extrapolations is indicated in Figure 3.

For solutions containing more than one organic component, the contribution in volume weighted refractive index of each solute, *i*, was considered separately:

$$RI_{org} = \frac{1}{V_{org}} \sum_{i} RI_{i}V_{i} \quad (3)$$

$$V_{f,org} = \frac{RI_{drop} - RI_{w}}{\frac{1}{V_{org}} \sum_{i} RI_{i}V_{i} - RI_{w}} \quad (4)$$

For both binary and multicomponent aerosol, a value of D_0 was determined from the particle radius and refractive index pairing retrieved from the Raman spectra at every RH step, with the mean and standard deviation of these values then taken to give an average value for D_0, along with an associated error, σ. The mean value of D_0 was used to convert measured wet size to a *GF*, with this then used in equation (1) to determine a value of κ for the organic compound at each a_w for which measurements were taken. Upper and lower bounds were placed on the retrieved κ values by performing the same calculation using dry particle diameters of $D_0 \pm \sigma$ to calculate the GFs.

II.b Electrodynamic Balance Measurements

The equilibrium hygroscopic properties of aerosol play a key role in the mass transfer dynamics of water between the droplet and gas phase.[60] Indeed, we have shown that measurements of the evaporation rate of water from aerosol droplets of known composition may be used to determine hygroscopic growth of aerosol

at water activities approaching saturation.[61] We use the same approach here and only briefly review the technique. Using an electrodynamic balance held at a fixed RH and temperature, measurements of water evaporation from aerosol droplets of two compositions were rapidly studied in sequence, introducing the droplets from two droplet-on-demand micro-dispensers (Figure 4a). Following the evaporation of a pure water droplet, which was used as a probe/control for determining the gas phase conditions, a droplet containing a sample solute was introduced and its approach to equilibrium monitored. The time-dependencies in droplet radii were determined with 10 ms time-resolution from the angular fringe spacing in the elastic scattering pattern using a geometrical optic approximation.[62] Changes in refractive index were accounted for in a post-analysis step,[63] and the average evaporation trends for multiple droplets of both probe and sample solutions were found.

The evaporation rate of pure water from the control droplet was used to estimate the RH in the gas phase, using the equations of Kulmala et al. to simulate the evaporation kinetics, with an accuracy in the gas phase water activity of around ±0.001 at 0.95 and ± 0.003 at 0.90.[64,65] The evaporation of the sample solution droplets took place under identical conditions given the timescales of the measurements. A simple volume additive approach to treating the solution density was employed to determine the mass flux at every time resolved radius and, from estimates of the initial size and mass concentration, a dry size was determined and a growth factor at every radius deduced (Figure 4b (inset)). Under the assumption that gas phase diffusion was the limiting process in evaporation (a valid assumption given the insensitivities to surface processes and the non-viscous nature of the particles),[60] the equations of Kulmala et al. were used to calculate, using the RH and mass flux, the water activity of the droplet at every size. The results of this procedure were averaged and are shown against growth factor in Figure 4b. This procedure has been demonstrated in our previous work[61] and is used here as a way of determining hygroscopicity at water activities approaching unity. The sensitivity of the droplet evaporation measurements to different values of κ is illustrated in Figure 5(a), clearly indicating the differences in hygroscopicity which can be resolved by the comparative kinetic technique. For comparison, the evaporation profiles for two compounds with different values of κ are shown in Figure 5(b). These are intended only as examples and it should be noted that the two measurements are into marginally different RHs and the droplets follow different variations in density with composition.

250

251 **IV. RESULTS AND DISCUSSION**

252 In Figure 6 we report the experimentally determined κ values retrieved at different values of water activity
253 for selected compounds studied with varying O/C. Values estimated from both the AOT (with a_w between
254 0.55 - 0.8) and EDB (with $a_w > 0.9$) techniques are shown. As apparent from the data, the techniques are in
255 good agreement and provide consistent values of κ as the same a_w is approached, indicated by linear fits to
256 the data used to guide the eye. Although no increase in κ at very high water activity can be discerned within
257 experimental error as infinite dilution is approached, an increase in the apparent κ is observed as the RH/a_w
258 decreases. The retrieval of an apparent dependence of κ on a_w provides a clear demonstration of the
259 limitations of the κ-Köhler model at relative humidities below the dilute limit when solution non-ideality
260 becomes significant and the assumptions inherent to the theory no longer apply. The sensitivity of the κ
261 value to the a_w of the measurement varies from compound to compound, as demonstrated by the five
262 representative compounds shown in Figure 6. The κ values determined from the EDB measurements show
263 excellent self-consistency over the limited range of high a_w measurements.

264

265 A single value of κ was determined from the AOT measurements by calculating the *GF* at the highest
266 measured RH and converting it using the κ-Köhler equation. An associated uncertainty was derived from the
267 uncertainty in the pure organic refractive index (from the extrapolation in Figure 3) and the standard
268 deviation of the dry size. Single values of κ were determined from the EDB measurements by averaging over
269 the values determined at each a_w, with the uncertainty then given by the standard deviation in these values.
270 We summarise the values estimated from the AOT and EDB measurements in Figure 7 and Table 1: a clear
271 general trend of increasing hygroscopicity with increasing O/C is observed, consistent with previous
272 observations.[7,53,66–69]

273

274 We have undertaken an extensive review of κ values published in the literature (also shown in Figure 7)
275 encompassing a wide range of measurements that have included ensemble field measurements, chamber
276 SOA studies, and single particle measurements, which have yielded data for multicomponent atmospheric
277 aerosol, analogous laboratory-generated systems, and individual pure component particles, respectively (see

Supplementary Information, Table 1). The measurement techniques used to determine κ can be divided according to those operating in the subsaturated regime (RH < 100 %) and in the supersaturated regime (RH > 100 %). In the subsaturated regime, the majority of literature studies used an HTDMA to determine the hygroscopic properties of ensemble aerosol.[5–7,18–20,69–75] Other subsaturated techniques that have been used included aerosol optical tweezers,[8] electrodynamic balances,[9–11] cavity ring down spectroscopy,[68] a differential aerosol sizing and hygroscopicity spectrometer probe (DASH-SP),[76,77] the Leipzig Aerosol Cloud Interaction Simulator (LACIS),[78] and a continuous-flow thermal gradient column (CFTGC).[52] Measurements in the supersaturated regime were mostly performed used a cloud condensation nuclei counter (CCNC), inferring the hygroscopicity parameter from critical supersaturations.[18,19,53,66,67,75,79–89] In this technique, a narrow size fraction of the aerosol sample to be studied is selected using, for example, a DMA or a virtual impactor and exposed to a chosen supersaturation. The ratio of the number of aerosol particles that activate to the total number of particles exposed to the supersaturation is then calculated. By scanning through different supersaturations, the critical supersaturation is determined as the value at which 50 % of the aerosol particles activate, which can then be used to estimate κ. In the vast majority of the literature studies, the O/C for the aerosol was determined from aerosol mass spectrometer (AMS) f_{44} values according to the Aiken et al. parameterisation.[5–7,20,53,66–69,71–73,75–85,87–89] In other cases the chemical composition of the aerosol was well defined and thus the O/C was calculated from the molecular formula.[8–11,18,19,52,70,74,86] The published studies found in the literature reported κ values for aerosols with O/C ranging from around 0 to 2.

The data identified in the literature review show a general positive correlation between κ and O/C, although it is not possible to represent the relationship between κ and O/C with a simple linear parameterisation (Figure 7). In order to identify whether specific measurement regimes or types of aerosol sample could lead to systematic variations in the value of κ, the literature data have been subdivided in three ways: a) according to the saturation regime under which it was taken, b) the origin of the aerosol sample, and c) the method by which the O/C was determined. These three divisions are shown as separate panels in Figure 8. It is clear that regardless of the criterion used to divide the data, equivalent levels of variability in the value of κ for a given O/C are observed from the literature data. Although the O/C ratio is a frequently used measure of aerosol composition/age, Figures 7 and 8 suggest that it is a poor indicator of hygroscopicity. This conclusion is

306 supported by the AOT and EDB measurements reported in this study, which mirror closely the degree of
307 scatter seen in the literature data, in particular the large variation in the value of κ seen in the measurements
308 for O/C = 1.
309
310 It is instructive to consider how the scatter in the values of κ at a given O/C would manifest itself as an
311 uncertainty in the predicted critical supersaturation for CCN activation if a linear parameterisation linking κ
312 and O/C was used to calculate this quantity. Figure 9a shows all of the data points presented in Figure 7
313 binned according to their O/C in intervals of 0.1, with the κ values taken as the average of all data points in
314 each O/C bin and the error bars showing the associated standard deviation. Any uncertainties in the κ values
315 reported in the original studies have been ignored and we consider only the minimum error that would be
316 introduced in to the critical supersaturation by use of a linear κ to O/C parameterisation. The grey shaded
317 region on Figure 9a indicates the uncertainty envelope for the linear best fit through both the literature and
318 new experimental κ data reported in this manuscript. The line of best fit is weighted by the standard
319 deviations at each O/C ratio. Also shown for comparison are two previously proposed sets of linear
320 parameterisations,[7,53] which have been extrapolated to cover the same O/C range as the present study. The
321 previous parameterisations are significantly different in gradient from that determined from the average of
322 the available literature data, reflecting the much smaller data sets, limited range of organic species and
323 narrower O/C ranges on which they were based. A similar data binning and fitting procedure was also
324 performed for each of the data sub-sets (6 cases) identified in Figure 8 (Supplementary information Figure 1
325 and Table 2). Although the uncertainties in the correlations is much lower for aerosol of known composition
326 measured in the laboratory, as might be expected, the spread in the fitted correlations is such that no
327 definitive conclusions can be made from the comparison of sub-saturated growth and critical supersaturation
328 measurements.
329
330 In Figure 9b we report the sensitivity of the predicted critical supersaturations to the value of κ derived at
331 varying O/C from the different parameterisations shown in Figure 9a. The spread in the κ values from the
332 literature survey for aerosol of a particular O/C, ignoring experimental errors, leads to a spread in the
333 predicted critical supersaturations. Considering the data point at O/C = 0.56 in Figure 9b alone, the spread in

critical supersaturation arising from the error bar at this O/C ratio is –17 % to +34 % on a critical supersaturation of 0.36 % RH (where this is the value from a κ of 0.10 ± 0.05). This is equivalent to a range of 0.30 to 0.48 % RH in critical supersaturation for an activating particle of 100 nm diameter and is larger than typical uncertainties in experimentally determined supersaturations, which are of the order ±0.04 % RH.[53] However, the uncertainty in the new parameterisation provided here from fitting all of the literature data over the whole O/C range yields uncertainties in the critical supersaturation that are comparable to the errors associated with experimental measurements of supersaturations. Again at an O/C ratio of 0.56, the spread in critical supersaturations shown in Figure 9b is 0.33 to 0.43 % for a particle of 100 nm diameter. The envelope defining the parameterisation is:

$$\kappa = (0.190 \pm 0.017) \times (O/C) - (0.0048 \pm 0.0139) \quad (5)$$

As a further sensitivity test, Figure 10 shows the uncertainty in critical supersaturation with O/C for particles of three different diameters that would result from the uncertainty in the parameterisation of the dependence of κ on O/C shown in Figure 9. CCN of different dry size become virtually indistinguishable in terms of their critical supersaturation when they have a composition commensurate with low O/C.

From Figures 9 and 10, it can be concluded that a general parameterisation of the dependence of κ on O/C, such as that shown by the grey envelope in Figure 9a, can provide an approximate yet appropriate indicator of the critical supersaturation and hygroscopic growth. Notably the variation in critical supersaturations predicted by the different parameterisations for the O/C dependence of κ is considerably larger than identified by the grey shaded envelope in Figure 9a. Given that the different parameterisations are based on measurements performed on aerosols of different organic precursor type and oxidation mechanism, the disparity between them does suggest that more accurate treatments of hygroscopic growth and CCN activation must rely on different parameterisations for different chemical systems.

V. SUMMARY

We have reported new measurements of the hygroscopicity parameter κ for chemical compounds with a range of O/C values and differing chemical functionalities. Measurements were made on single aerosol particles using aerosol optical tweezers and an electrodynamic balance, with excellent agreement seen

between the two techniques. As the RH was decreased, deviation in the apparent κ from the constant value seen at high a_w was observed, highlighting the need to make measurements of κ at high a_w in the dilute limit where ideality can be assumed. The variation in the hygroscopicity parameter κ between compounds of even the same O/C ratio is found to be significant with, for example, a range in κ values from 0.12 to 0.38 for compounds with an O/C of 1.

A comprehensive review of all κ values published in the literature to date along with their associated O/C ratios has been undertaken, encompassing field and laboratory studies, subsaturated and supersaturated measurements, and multi-component and pure component aerosol. The literature data, combined with the newly determined experimental values, showed a general positive correlation between κ and O/C, in qualitative agreement with previously published results. We have presented a linear parameterisation of the correlation between κ and O/C based on all of the published data for which both the κ value and O/C ratio are known, showing a somewhat weaker dependence of κ on O/C than previous parameterisations. The uncertainty in the predicted value of κ resulting from this parameterisation leads to an uncertainty in the predicted critical supersaturation that is very similar to typical uncertainties associated with experimental measurements of critical supersaturations. However, it should be stressed that significant variations are observed between the κ *vs* O/C parameterisations derived from measurements with different aerosol types, suggesting that the chemical complexity of a species hygroscopic response cannot be reliably captured by a single parameter such as O/C.

ACKNOWLEDGEMENTS

We thank the Engineering and Physical Sciences Research Council for financial support through a Leadership Fellowship awarded to JPR (grant reference EP/G007713/1). REHM acknowledges the National Environmental Research Council for financial support (grant reference NE/1020075/1). Drs. Thomas Preston and Jim Walker are acknowledge at the latter stages of this project for developing new software to determine the size and refractive index of optically trapped droplets.

Supporting Information Available

Details of the literature review of hygroscopicity studies that report values of κ are given in the Supporting Information, along with the additional fits described in Section IV. This information is available free of charge via the Internet at http://pubs.acs.org

REFERENCES

(1) Twomey, S. The Influence of Pollution on the Shortwave Albedo of Clouds. *J. Atmos. Sci.* **1977**, *34*, 1149–1152.

(2) Albrecht, B. A. Aerosols, Cloud Microphysics, and Fractional Cloudiness. *Science* **1989**, *245*, 1227–1230.

(3) Kanakidou, M.; Seinfeld, J. H.; Pandis, S. N.; Barnes, I.; Dentener, F. J.; Facchini, M. C.; Van Dingenen, R.; Ervens, B.; Nenes, A.; Nielsen, C. J. et al. Organic Aerosol and Global Climate Modelling: a Review. *Atmos. Chem. Phys.* **2005**, *5*, 1053–1123.

(4) Forster, P.; Ramaswamy, V.; Artaxo, P.; Berntsen, T.; Betts, R.; Fahey, D. W. 2007: Changes in Atmospheric Constituents and in Radiative Forcing. In *Climate Change 2007: The Physical Science Basis. Contribution of Working Group I to the Fourth Assessment Report of the Intergovernmental Panel on Climate Change*; 2007; pp. 129–234.

(5) Alfarra, M. R.; Hamilton, J. F.; Wyche, K. P.; Good, N.; Ward, M. W.; Carr, T.; Barley, M. H.; Monks, P. S.; Jenkin, M. E.; Lewis, A. C. et al. The Effect of Photochemical Ageing and Initial Precursor Concentration on the Composition and Hygroscopic Properties of B-caryophyllene Secondary Organic Aerosol. *Atmos. Chem. Phys.* **2012**, *12*, 6417–6436.

(6) Liu, Y.; Monod, A.; Tritscher, T.; Praplan, A. P.; DeCarlo, P. F.; Temime-Roussel, B.; Quivet, E.; Marchand, N.; Dommen, J.; Baltensperger, U. Aqueous Phase Processing of Secondary Organic Aerosol from Isoprene Photooxidation. *Atmos. Chem. Phys.* **2012**, *12*, 5879–5895.

(7) Duplissy, J.; DeCarlo, P. F.; Dommen, J.; Alfarra, M. R.; Metzger, A.; Barmpadimos, I.; Prevot, A. S. H.; Weingartner, E.; Tritscher, T.; Gysel, M. et al. Relating Hygroscopicity and Composition of Organic Aerosol Particulate Matter. *Atmos. Chem. Phys.* **2011**, *11*, 1155–1165.

(8) Dennis-Smither, B. J.; Hanford, K. L.; Kwamena, N.-O. A.; Miles, R. E. H.; Reid, J. P. Phase, Morphology, and Hygroscopicity of Mixed Oleic Acid/sodium Chloride/water Aerosol Particles Before and After Ozonolysis. *J. Phys. Chem. A* **2012**, *116*, 6159–68.

(9) Chan, M. N.; Kreidenweis, S. M.; Chan, C. K. Measurements of the Hygroscopic and Deliquescence Properties of Organic Compounds of Different Solubilities in Water and Their Relationship with Cloud Condensation Nuclei Activities. *Environ. Sci. Technol.* **2008**, *42*, 3602–8.

(10) Pope, F. D.; Tong, H.-J.; Dennis-Smither, B. J.; Griffiths, P. T.; Clegg, S. L.; Reid, J. P.; Cox, R. A. Studies of Single Aerosol Particles Containing Malonic Acid, Glutaric Acid, and Their Mixtures with Sodium Chloride. II. Liquid-State Vapor Pressures of the Acids. *J. Phys. Chem. A* **2010**, *114*, 10156–10165.

(11) Pope, F. D.; Harper, L.; Dennis-Smither, B. J.; Griffiths, P. T.; Clegg, S. L.; Cox, R. A. Laboratory and Modelling Study of the Hygroscopic Properties of Two Model Humic Acid Aerosol Particles. *J. Aerosol Sci.* **2010**, *41*, 457–467.

(12) Clegg, S. L.; Brimblecombe, P.; Wexler, A. S. Thermodynamic Model of the System H+−NH4+−Na+−SO42-−NO3-−Cl-−H2O at 298.15 K. *J. Phys. Chem. A* **1998**, *102*, 2155–2171.

(13) Peng, C.; Chan, M. N.; Chan, C. K. The Hygroscopic Properties of Dicarboxylic and Multifunctional Acids: Measurements and UNIFAC Predictions. *Environ. Sci. Technol.* **2001**, *35*, 4495–501.

(14) Wexler, A. S.; Clegg, S. L. Atmospheric Aerosol Models for Systems Including the Ions H+, NH4+, Na+, SO42-, NO3-, Cl-, Br-, and H2O. *J. Geophys. Res.* **2002**, *107*.

(15) Topping, D. O.; McFiggans, G. B.; Coe, H. A Curved Multi-component Aerosol Hygroscopicity Model Framework: Part 1 – Inorganic Compounds. *Atmos. Chem. Phys.* **2005**, *5*, 1205–1222.

(16) Zuend, A.; Marcolli, C.; Luo, B. P.; Peter, T. A Thermodynamic Model of Mixed Organic-inorganic Aerosols to Predict Activity Coefficients. *Atmos. Chem. Phys.* **2008**, *8*, 4559–4593.

(17) Zuend, A.; Marcolli, C.; Booth, A. M.; Lienhard, D. M.; Soonsin, V.; Krieger, U. K.; Topping, D. O.; McFiggans, G.; Peter, T.; Seinfeld, J. H. New and Extended Parameterization of the Thermodynamic Model AIOMFAC: Calculation of Activity Coefficients for Organic-inorganic Mixtures Containing Carboxyl, Hydroxyl, Carbonyl, Ether, Ester, Alkenyl, Alkyl, and Aromatic Functional Groups. *Atmos. Chem. Phys.* **2011**, *11*, 9155–9206.

(18) Petters, M. D.; Kreidenweis, S. M. A Single Parameter Representation of Hygroscopic Growth and Cloud Condensation Nucleus Activity. *Atmos. Chem. Phys.* **2007**, *7*, 1961–1971.

(19) Petters, M. D.; Kreidenweis, S. M.; Prenni, A. J.; Sullivan, R. C.; Carrico, C. M.; Koehler, K. A.; Ziemann, P. J. Role of Molecular Size in Cloud Droplet Activation. *Geophys. Res. Lett.* **2009**, *36*, L22801.

(20) Jimenez, J. L.; Canagaratna, M. R.; Donahue, N. M.; Prevot, A. S. H.; Zhang, Q.; Kroll, J. H.; DeCarlo, P. F.; Allan, J. D.; Coe, H.; Ng, N. L. et al. Evolution of Organic Aerosols in the Atmosphere. *Science* **2009**, *326*, 1525–9.

(21) Zhang, Q.; Jimenez, J. L.; Canagaratna, M. R.; Allan, J. D.; Coe, H.; Ulbrich, I.; Alfarra, M. R.; Takami, A.; Middlebrook, A. M.; Sun, Y. L. et al. Ubiquity and Dominance of Oxygenated Species in Organic Aerosols in Anthropogenically-influenced Northern Hemisphere Midlatitudes. *Geophys. Res. Lett.* **2007**, *34*, L13801.

(22) Jacobson, M. C.; Hansson, H.-C.; Noone, K. J.; Charlson, R. J. Organic Atmospheric Aerosols: Review and State of the Science. *Rev. Geophys.* **2000**, *38*, 267.

(23) Saxena, P.; Hildemann, L. M. Water-Soluble Organics in Atmospheric Particles : A Critical Review of the Literature and Application of Thermodynamics to Identify Candidate Compounds. *J. Atmos. Chem.* **1996**, *24*, 57–109.

(24) Topping, D.; Connolly, P.; McFiggans, G. Cloud Droplet Number Enhanced by Co-condensation of Organic Vapours. *Nat. Geosci.* **2013**, *6*, 443–446.

(25) You, Y.; Renbaum-Wolff, L.; Carreras-Sospedra, M.; Hanna, S. J.; Hiranuma, N.; Kamal, S.; Smith, M. L.; Zhang, X.; Weber, R. J.; Shilling, J. E. et al. Images Reveal That Atmospheric Particles Can Undergo Liquid-liquid Phase Separations. *Proc. Natl. Acad. Sci. USA* **2012**, *109*, 13188–93.

(26) Ruehl, C. R.; Chuang, P. Y.; Nenes, A.; Cappa, C. D.; Kolesar, K. R.; Goldstein, A. H. Strong Evidence of Surface Tension Reduction in Microscopic Aqueous Droplets. *Geophys. Res. Lett.* **2012**, *39*.

(27) Stokes, R. H.; Robinson, R. A. Interactions in Aqueous Nonelectrolyte Solutions. I. Solute-Solvent Equilibria. *J. Phys. Chem.* **1966**, *70*, 2126–2131.

(28) Petters, M. D.; Kreidenweis, S. M. A Single Parameter Representation of Hygroscopic Growth and Cloud Condensation Nucleus Activity – Part 3: Including Surfactant Partitioning. *Atmos. Chem. Phys.* **2013**, *13*, 1081–1091.

(29) Vestin, A.; Rissler, J.; Swietlicki, E.; Frank, G. P.; Andreae, M. O. Cloud-nucleating Properties of the Amazonian Biomass Burning Aerosol: Cloud Condensation Nuclei Measurements and Modeling. *J. Geophys. Res.* **2007**, *112*, D14201.

(30) Wex, H.; Hennig, T.; Salma, I.; Ocskay, R.; Kiselev, A.; Henning, S.; Massling, A.; Wiedensohler, A.; Stratmann, F. Hygroscopic Growth and Measured and Modeled Critical Super-saturations of an Atmospheric HULIS Sample. *Geophys. Res. Lett.* **2007**, *34*, L02818.

(31) Carrico, C. M.; Petters, M. D.; Kreidenweis, S. M.; Collett, J. L.; Engling, G.; Malm, W. C. Aerosol Hygroscopicity and Cloud Droplet Activation of Extracts of Filters from Biomass Burning Experiments. *J. Geophys. Res.* **2008**, *113*, D08206.

(32) Duplissy, J.; Gysel, M.; Alfarra, M. R.; Dommen, J.; Metzger, A.; Prevot, A. S. H.; Weingartner, E.; Laaksonen, A.; Raatikainen, T.; Good, N. et al. Cloud Forming Potential of Secondary Organic Aerosol Under Near Atmospheric Conditions. *Geophys. Res. Lett.* **2008**, *35*, 1–5.

(33) Petters, M. D.; Carrico, C. M.; Kreidenweis, S. M.; Prenni, A. J.; DeMott, P. J.; Collett, J. L.; Moosmüller, H. Cloud Condensation Nucleation Activity of Biomass Burning Aerosol. *J. Geophys. Res.* **2009**, *114*, D22205.

(34) Mochida, M.; Nishita-Hara, C.; Kitamori, Y.; Aggarwal, S. G.; Kawamura, K.; Miura, K.; Takami, A. Size-segregated Measurements of Cloud Condensation Nucleus Activity and Hygroscopic Growth for Aerosols at Cape Hedo, Japan, in Spring 2008. *J. Geophys. Res.* **2010**, *115*, D21207.

(35) Wex, H.; Fuentes, E.; Tsagkogeorgas, G.; Voigtländer, J.; Clauss, T.; Kiselev, A.; Green, D. H.; Coe, H.; McFiggans, G.; Stratmann, F. The Influence of Algal Exudate on the Hygroscopicity of Sea Spray Particles. *Adv. Meteor.* **2010**, *2010*, 1–11.

(36) Engelhart, G. J.; Nenes, A.; Pandis, S. N. CCN Activity and Droplet Growth Kinetics of Fresh and Aged Monoterpene Secondary Organic Aerosol. *Atmos. Chem. Phys.* **2008**, *8*, 3937–3949.

(37) Moore, R. H.; Ingall, E. D.; Sorooshian, A.; Nenes, A. Molar Mass, Surface Tension, and Droplet Growth Kinetics of Marine Organics from Measurements of CCN Activity. *Geophys. Res. Lett.* **2008**, *35*.

(38) King, S. M.; Rosenoern, T.; Shilling, J. E.; Chen, Q.; Martin, S. T. Increased Cloud Activation Potential of Secondary Organic Aerosol for Atmospheric Mass Loadings. *Atmos. Chem. Phys.* **2009**, *9*, 2959–2972.

(39) Wex, H.; Petters, M. D.; Carrico, C. M.; Hallbauer, E.; Massling, A.; Mcmeeking, G. R.; Poulain, L.; Wu, Z. Towards Closing the Gap Between Hygroscopic Growth and Activation for Secondary Organic Aerosol : Part 1 – Evidence from Measurements. *Atmos. Chem. Phys.* **2009**, *9*, 3987–3997.

(40) Good, N.; Topping, D. O.; Allan, J. D.; Flynn, M.; Fuentes, E.; Irwin, M.; Williams, P. I.; Coe, H. Consistency Between Parameterisations of Aerosol Hygroscopicity and CCN Activity During the RHaMBLe Discovery Cruise. *Atmos. Chem. Phys.* **2010**, *10*, 3189–3203.

(41) Irwin, M.; Good, N.; Crosier, J.; Choularton, T. W.; McFiggans, G. Reconciliation of Measurements of Hygroscopic Growth and Critical Supersaturation of Aerosol Particles in Central Germany. *Atmos. Chem. Phys.* **2010**, *10*, 11737–11752.

(42) Padró, L. T.; Tkacik, D.; Lathem, T.; Hennigan, C. J.; Sullivan, A. P.; Weber, R. J.; Huey, L. G.; Nenes, A. Investigation of Cloud Condensation Nuclei Properties and Droplet Growth Kinetics of the Water-soluble Aerosol Fraction in Mexico City. *J. Geophys. Res.* **2010**, *115*, D09204.

(43) Prenni, A. J.; Petters, M. D.; Kreidenweis, S. M.; DeMott, P. J.; Ziemann, P. J. Cloud Droplet Activation of Secondary Organic Aerosol. *J. Geophys. Res.* **2007**, *112*.

(44) Petters, M. D.; Wex, H.; Carrico, C. M.; Hallbauer, E.; Massling, A.; Mcmeeking, G. R.; Poulain, L.; Wu, Z. Towards Closing the Gap Between Hygroscopic Growth and Activation for Secondary Organic Aerosol – Part 2 : Theoretical Approaches. *Atmos. Chem. Phys.* **2009**, *9*, 3999–4009.

(45) Sjogren, S.; Gysel, M.; Weingartner, E.; Baltensperger, U.; Cubison, M. J.; Coe, H.; Zardini, A. A.; Marcolli, C.; Krieger, U. K.; Peter, T. Hygroscopic Growth and Water Uptake Kinetics of Two-phase Aerosol Particles Consisting of Ammonium Sulfate, Adipic and Humic Acid Mixtures. *J. Aerosol Sci.* **2007**, *38*, 157–171.

(46) Good, N.; Topping, D. O.; Duplissy, J.; Gysel, M.; Meyer, N. K.; Metzger, A.; Turner, S. F.; Baltensperger, U.; Ristovski, Z.; Weingartner, E. et al. Widening the Gap Between Measurement and Modelling of Secondary Organic Aerosol Properties? *Atmos. Chem. Phys.* **2010**, *10*, 2577–2593.

(47) Petters, M. D.; Kreidenweis, S. M. A Single Parameter Representation of Hygroscopic Growth and Cloud Condensation Nucleus Activity – Part 2 : Including Solubility. *Atmos. Chem. Phys.* **2008**, *8*, 5939–5955.

(48) Duplissy, J.; Gysel, M.; Sjogren, S.; Meyer, N.; Good, N.; Kammermann, L.; Michaud, V.; Weigel, R.; Martins dos Santos, S.; Gruening, C. et al. Intercomparison Study of Six HTDMAs: Results and Recommendations. *Atmos. Meas. Tech.* **2009**, *2*, 363–378.

(49) Rose, D.; Gunthe, S. S.; Mikhailov, E.; Frank, G. P.; Dusek, U.; Andreae, M. O. Calibration and Measurement Uncertainties of a Continuous-flow Cloud Condensation Nuclei Counter (DMT-CCNC): CCN Activation of Ammonium Sulfate and Sodium Chloride Aerosol Particles in Theory and Experiment. *Atmos. Chem. Phys.* **2008**, *8*, 1153–1179.

(50) Walker, J. S.; Wills, J. B.; Reid, J. P.; Wang, L.; Topping, D. O.; Butler, J. R.; Zhang, Y.-H. Direct Comparison of the Hygroscopic Properties of Ammonium Sulfate and Sodium Chloride Aerosol at Relative Humidities Approaching Saturation. *J. Phys. Chem. A* **2010**, *114*, 12682–91.

(51) Fredenslund, A.; Jones, R. L.; Prausnitz, J. M. Group-Contribution Estimation of Activity Coefficients in Nonideal Liquid Mixtures. *AIChE J.* **1975**, *21*, 1086–1099.

(52) Ruehl, C. R.; Chuang, P. Y.; Nenes, A. Aerosol Hygroscopicity at High (99 to 100%) Relative Humidities. *Atmos. Chem. Phys.* **2010**, *10*, 1329–1344.

(53) Chang, R. Y.-W.; Slowik, J. G.; Shantz, N. C.; Vlasenko, A.; Liggio, J.; Sjostedt, S. J.; Leaitch, W. R.; Abbatt, J. P. D. The Hygroscopicity Parameter (κ) of Ambient Organic Aerosol at a Field Site Subject to Biogenic and Anthropogenic Influences: Relationship to Degree of Aerosol Oxidation. *Atmos. Chem. Phys.* **2010**, *10*, 5047–5064.

(54) Aiken, A. C.; Decarlo, P. F.; Kroll, J. H.; Worsnop, D. R.; Huffman, J. A.; Docherty, K. S.; Ulbrich, I. M.; Mohr, C.; Kimmel, J. R.; Sueper, D. et al. O/C and OM/OC Ratios of Primary, Secondary, and Ambient Organic Aerosols with High-resolution Time-of-flight Aerosol Mass Spectrometry. *Environ. Sci. Technol.* **2008**, *42*, 4478–85.

(55) Dennis-Smither, B. J.; Miles, R. E. H.; Reid, J. P. Oxidative Aging of Mixed Oleic Acid/sodium Chloride Aerosol Particles. *J. Geophys. Res., [Atmos.]* **2012**, *117*.

(56) Hanford, K. L.; Mitchem, L.; Reid, J. P.; Clegg, S. L.; Topping, D. O.; McFiggans, G. B. Comparative Thermodynamic Studies of Aqueous Glutaric Acid, Ammonium Sulfate and Sodium Chloride Aerosol at High Humidity. *J. Phys. Chem. A* **2008**, *112*, 9413–22.

(57) Hargreaves, G.; Kwamena, N.-O. A.; Zhang, Y. H.; Butler, J. R.; Rushworth, S.; Clegg, S. L.; Reid, J. P. Measurements of the Equilibrium Size of Supersaturated Aqueous Sodium Chloride Droplets at Low Relative Humidity Using Aerosol Optical Tweezers and an Electrodynamic Balance. *J. Phys. Chem. A* **2010**, *114*, 1806–15.

(58) Miles, R. E. H.; Walker, J. S.; Burnham, D. R.; Reid, J. P. Retrieval of the Complex Refractive Index of Aerosol Droplets from Optical Tweezers Measurements. *Phys. Chem. Chem. Phys.* **2012**, *14*, 3037–3047.

(59) Preston, T. C.; Reid, J. P. Accurate and Efficient Determination of the Radius, Refractive Index and Dispersion of a Weakly Absorbing Spherical Particle Using Whispering Gallery Modes. *J. Opt. Soc. Am. B* **2013**, *In Press*.

(60) Davies, J. F.; Haddrell, A. E.; Miles, R. E. H.; Bull, C. R.; Reid, J. P. Bulk, Surface, and Gas-phase Limited Water Transport in Aerosol. *J. Phys. Chem. A* **2012**, *116*, 10987–98.

(61) Davies, J. F.; Haddrell, A. E.; Rickards, A. M. J.; Reid, J. P. Simultaneous Analysis of the Equilibrium Hygroscopicity and Water Transport Kinetics of Liquid Aerosol. *Anal. Chem.* **2013**.

(62) Glantschnig, W. J.; Chen, S. H. Light Scattering from Water Droplets in the Geometrical Optics Approximation. *Appl. Opt.* **1981**, *20*, 2499–509.

(63) Davies, J. F.; Haddrell, A. E.; Reid, J. P. Time-Resolved Measurements of the Evaporation of Volatile Components from Single Aerosol Droplets. *Aerosol Sci. Technol.* **2012**, *46*, 666–677.

(64) Kulmala, M.; Vesala, T.; Wagner, P. E. An Analytical Expression For the Rate of Binary Condensational Particle Growth. *Proc. R. Soc. Lond. A* **1993**, *441*, 589–605.

(65) Miles, R. E. H.; Reid, J. P.; Riipinen, I. Comparison of Approaches for Measuring the Mass Accommodation Coefficient for the Condensation of Water and Sensitivities to Uncertainties in Thermophysical Properties. *J. Phys. Chem. A* **2012**, *116*, 10810–25.

(66) Lambe, A. T.; Onasch, T. B.; Massoli, P.; Croasdale, D. R.; Wright, J. P.; Ahern, A. T.; Williams, L. R.; Worsnop, D. R.; Brune, W. H.; Davidovits, P. Laboratory Studies of the Chemical Composition and Cloud Condensation Nuclei (CCN) Activity of Secondary Organic Aerosol (SOA) and Oxidized Primary Organic Aerosol (OPOA). *Atmos. Chem. Phys.* **2011**, *11*, 8913–8928.

(67) Wong, J. P. S.; Lee, A. K. Y.; Slowik, J. G.; Cziczo, D. J.; Leaitch, W. R.; Macdonald, A.; Abbatt, J. P. D. Oxidation of Ambient Biogenic Secondary Organic Aerosol by Hydroxyl Radicals: Effects on Cloud Condensation Nuclei Activity. *Geophys. Res. Lett.* **2011**, *38*, L22805.

(68) Cappa, C. D.; Che, D. L.; Kessler, S. H.; Kroll, J. H.; Wilson, K. R. Variations in Organic Aerosol Optical and Hygroscopic Properties Upon Heterogeneous OH Oxidation. *J. Geophys. Res.* **2011**, *116*, 1–12.

(69) Mihara, T.; Mochida, M. Characterization of Solvent-extractable Organics in Urban Aerosols Based on Mass Spectrum Analysis and Hygroscopic Growth Measurement. *Environ. Sci. Technol.* **2011**, *45*, 9168–74.

(70) Hasenkopf, C. A.; Freedman, M. A.; Beaver, M. R.; Toon, O. B.; Tolbert, M. A. Potential Climatic Impact of Organic Haze on Early Earth. *Astrobiology* **2011**, *11*, 135–49.

(71) Tritscher, T.; Dommen, J.; DeCarlo, P. F.; Gysel, M.; Barmet, P. B.; Praplan, A. P.; Weingartner, E.; Prévôt, A. S. H.; Riipinen, I.; Donahue, N. M. et al. Volatility and Hygroscopicity of Aging Secondary Organic Aerosol in a Smog Chamber. *Atmos. Chem. Phys.* **2011**, *11*, 11477–11496.

(72) Tritscher, T.; Jurányi, Z.; Martin, M.; Chirico, R.; Gysel, M.; Heringa, M. F.; DeCarlo, P. F.; Sierau, B.; Prévôt, A. S. H.; Weingartner, E. et al. Changes of Hygroscopicity and Morphology During Ageing of Diesel Soot. *Environ. Res. Lett.* **2011**, *6*, 034026.

(73) Massoli, P.; Lambe, A. T.; Ahern, A. T.; Williams, L. R.; Ehn, M.; Mikkilä, J.; Canagaratna, M. R.; Brune, W. H.; Onasch, T. B.; Jayne, J. T. et al. Relationship Between Aerosol Oxidation Level and Hygroscopic Properties of Laboratory Generated Secondary Organic Aerosol (SOA) Particles. *Geophys. Res. Lett.* **2010**, *37*, 1–5.

(74) Mikhailov, E.; Vlasenko, S.; Martin, S. T.; Koop, T. Amorphous and Crystalline Aerosol Particles Interacting with Water Vapor: Conceptual Framework and Experimental Evidence for Restructuring, Phase Transitions and Kinetic Limitations. *Atmos. Chem. Phys.* **2009**, *9*, 9491–9522.

(75) Lang-Yona, N.; Rudich, Y.; Mentel, T. F.; Bohne, A.; Buchholz, A.; Kiendler-Scharr, A.; Kleist, E.; Spindler, C.; Tillmann, R.; Wildt, J. The Chemical and Microphysical Properties of Secondary Organic Aerosols from Holm Oak Emissions. *Atmos. Chem. Phys.* **2010**, *10*, 7253–7265.

(76) Hersey, S. P.; Craven, J. S.; Schilling, K. A.; Metcalf, A. R.; Sorooshian, A.; Chan, M. N.; Flagan, R. C.; Seinfeld, J. H. The Pasadena Aerosol Characterization Observatory (PACO): Chemical and Physical Analysis of the Western Los Angeles Basin Aerosol. *Atmos. Chem. Phys.* **2011**, *11*, 7417–7443.

(77) Sorooshian, A.; Murphy, S. M.; Hersey, S.; Gates, H.; Padro, L. T.; Nenes, A.; Brechtel, F. J.; Jonsson, H.; Flagan, R. C.; Seinfeld, J. H. Comprehensive Airborne Characterization of Aerosol from a Major Bovine Source. *Atmos. Chem. Phys.* **2008**, *8*, 5489–5520.

(78) Poulain, L.; Wu, Z.; Petters, M. D.; Wex, H.; Hallbauer, E.; Wehner, B.; Massling, A.; Kreidenweis, S. M.; Stratmann, F. Towards Closing the Gap Between Hygroscopic Growth and CCN Activation for Secondary Organic Aerosols – Part 3: Influence of the Chemical Composition on the Hygroscopic Properties and Volatile Fractions of Aerosols. *Atmos. Chem. Phys.* **2010**, *10*, 3775–3785.

(79) Moore, R. H.; Raatikainen, T.; Langridge, J. M.; Bahreini, R.; Brock, C. A.; Holloway, J. S.; Lack, D. A.; Middlebrook, A. M.; Perring, A. E.; Schwarz, J. P. et al. CCN Spectra, Hygroscopicity, and Droplet Activation Kinetics of Secondary Organic Aerosol Resulting from the 2010 Deepwater Horizon Oil Spill. *Environ. Sci. Technol.* **2012**, *46*, 3093–100.

(80) Tang, X.; Zheng, Z.; Jung, H. S.; Asa-Awuku, A. The Effects of Mainstream and Sidestream Environmental Tobacco Smoke Composition for Enhanced Condensational Droplet Growth by Water Vapor. *Aerosol Sci. Technol.* **2012**, *46*, 760–766.

(81) Engelhart, G. J.; Moore, R. H.; Nenes, A.; Pandis, S. N. Cloud Condensation Nuclei Activity of Isoprene Secondary Organic Aerosol. *J. Geophys. Res.* **2011**, *116*, 1–11.

(82) Frosch, M.; Bilde, M.; DeCarlo, P. F.; Jurányi, Z.; Tritscher, T.; Dommen, J.; Donahue, N. M.; Gysel, M.; Weingartner, E.; Baltensperger, U. Relating Cloud Condensation Nuclei Activity and Oxidation Level of α -pinene Secondary Organic Aerosols. *J. Geophys. Res.* **2011**, *116*, D22212.

(83) Kuwata, M.; Chen, Q.; Martin, S. T. Cloud Condensation Nuclei (CCN) Activity and Oxygen-to-carbon Elemental Ratios Following Thermodenuder Treatment of Organic Particles Grown by A-pinene Ozonolysis. *Phys. Chem. Chem. Phys.* **2011**, *13*, 14571–83.

(84) Lambe, A. T.; Ahern, A. T.; Williams, L. R.; Slowik, J. G.; Wong, J. P. S.; Abbatt, J. P. D.; Brune, W. H.; Ng, N. L.; Wright, J. P.; Croasdale, D. R. et al. Characterization of Aerosol Photooxidation Flow Reactors: Heterogeneous Oxidation, Secondary Organic Aerosol Formation and Cloud Condensation Nuclei Activity Measurements. *Atmos. Meas. Tech.* **2011**, *4*, 445–461.

(85) Moore, R. H.; Bahreini, R.; Brock, C. A.; Froyd, K. D.; Cozic, J.; Holloway, J. S.; Middlebrook, A. M.; Murphy, D. M.; Nenes, A. Hygroscopicity and Composition of Alaskan Arctic CCN During April 2008. *Atmos. Chem. Phys.* **2011**, *11*, 11807–11825.

(86) Frosch, M.; Zardini, A. A.; Platt, S. M.; Müller, L.; Reinnig, M.-C.; Hoffmann, T.; Bilde, M. Thermodynamic Properties and Cloud Droplet Activation of a Series of Oxo-acids. *Atmos. Chem. Phys.* **2010**, *10*, 5873–5890.

(87) George, I. J.; Abbatt, J. P. D. Chemical Evolution of Secondary Organic Aerosol from OH-initiated Heterogeneous Oxidation. *Atmos. Chem. Phys.* **2010**, *10*, 5551–5563.

(88) King, S. M.; Rosenoern, T.; Shilling, J. E.; Chen, Q.; Wang, Z.; Biskos, G.; McKinney, K. A.; Pöschl, U.; Martin, S. T. Cloud Droplet Activation of Mixed Organic-sulfate Particles Produced by the Photooxidation of Isoprene. *Atmos. Chem. Phys.* **2010**, *10*, 3953–3964.

(89) Roberts, G. C.; Day, D. A.; Russell, L. M.; Dunlea, E. J.; Jimenez, J. L.; Tomlinson, J. M.; Collins, D. R.; Shinozuka, Y.; Clarke, A. D. Characterization of Particle Cloud Droplet Activity and Composition in the Free Troposphere and the Boundary Layer During INTEX-B. *Atmos. Chem. Phys.* **2010**, *10*, 6627–6644.

(90) Haynes, W. M. Section 5: Thermochemistry, Electrochemistry, and Kinetics. In *CRC Handbook of Chemistry and Physics*; pp. 154–189.

(91) Gaivoronskii, A. N.; Granzhan, V. A. Solubility of Adipic Acid in Organic Solvents and Water. *Russ. J. Appl. Chem.* **2005**, *78*, 404–408.

(92) Attané, E. C.; Doumani, T. F. Solubilities of Aliphatic Dicarboxylic Acids in Water. *Ind. Eng. Chem.* **1949**, 2015–2017.

(93) Higashiyama, T. Novel Functions and Applications of Trehalose. *Pure Appl. Chem.* **2002**, *74*, 1263–1269.

664 **TABLES**

665 Table 1: A list of organic compounds for which hygroscopic growth was determined. Solubility data are
666 taken from (a) the CRC Handbook of Chemistry and Physics,[90] (b) Gaivoronskii and Granzhan,[91] (c) Attané
667 and Doumani,[92] and (d) Higashiyama,[93] with the measurement temperature in superscript. All compounds
668 were sourced from Sigma-Aldrich, with the exception of glutaric acid (Acros Organics), maleic acid (Acros
669 Organics), and citric acid (Fisher Scientific). The experimental technique used to determine κ is given and
670 those values are presented in the final column along with the corresponding a_w.

Compound	O/C	Solubility by mass	Technique	κ ($a_w \pm 0.02$)
Oleic acid ($C_{18}H_{34}O_2$, >90 %)	0.11	-	AOT	0.003 ± 0.001 (0.60 - 0.75)
Adipic acid ($C_6H_{10}O_4$, ≥ 99.5 %)	0.67	1.8 %, b$^{20^\circ C}$	EDB	0.102 ± 0.009 (> 0.90)
Glutaric acid ($C_5H_8O_4$, 99 %)	0.80	51 %, c$^{18^\circ C}$	EDB	0.168 ± 0.030 (> 0.90)
D-(+)-Raffinose ($C_{18}H_{32}O_{16}$, ≥ 98.0 %)	0.89	12.5 %, a$^{20^\circ C}$	EDB	0.063 ± 0.012 (> (0.90)
Sucrose ($C_{12}H_{22}O_{11}$, ≥ 99.5 %)	0.92	67.1 %, a$^{20^\circ C}$	EDB	0.115 ± 0.005 (> 0.90)
D-(+)-Trehalose ($C_{12}H_{22}O_{11}$, ≥ 99 %)	0.92	68.9 %, d$^{20^\circ C}$	EDB	0.116 ± 0.014 (> 0.90)
L-Ascorbic Acid ($C_6H_8O_6$, ≥ 99.0 %)	1	25.2 %, a$^{25^\circ C}$	AOT	0.192 ± 0.064 (0.80)
D-(+)-Galactose ($C_6H_{12}O_6$, ≥ 99 %)	1	40.6 %, a$^{20^\circ C}$	AOT EDB	0.212 ± 0.045 (0.80) 0.192 ± 0.013 (> 0.90)
D-(+)-Glucose ($C_6H_{12}O_6$, ≥ 99.5 %)	1	45.0 %, a$^{15^\circ C}$	EDB	0.254 ± 0.015 (> 0.90)
Maleic acid ($C_4H_4O_4$, 99 %)	1	44.1 %, a$^{25^\circ C}$	EDB	0.367 ± 0.021 (> 0.90)
D-Sorbitol ($C_6H_{14}O_6$, ≥ 98 %)	1	41 %, a$^{20^\circ C}$	AOT EDB	0.184 ± 0.011 (0.77) 0.154 ± 0.003 (> 0.90)
Succinic acid ($C_4H_6O_4$, ≥ 99.0 %)	1	7.7 %, a$^{25^\circ C}$	EDB	0.216 ± 0.020 (> 0.90)
trans-Aconitic acid ($C_6H_6O_6$, 98 %)	1	20.9 %, a$^{25^\circ C}$	EDB	0.172 ± 0.010 (> 0.90)
D-(+)-Xylose ($C_5H_{10}O_5$, ≥ 99 %)	1	30 %, a$^{25^\circ C}$	AOT	0.179 ± 0.015 (0.78)
Citric acid ($C_6H_8O_7$, > 99.5 %)	1.17	59 %, a$^{20^\circ C}$	AOT	0.233 ± 0.035 (0.66)
Malonic acid ($C_3H_4O_4$, 99 %)	1.33	42.4 %, a$^{20^\circ C}$	EDB	0.292 ± 0.011 (> 0.90)
L-(+)-Tartaric acid ($C_4H_6O_6$, ≥ 99.5 %)	1.50	58 %, a$^{20^\circ C}$	EDB	0.220 ± 0.007 (> 0.90)
Oxalic acid ($C_2H_2O_4$, ≥ 99.0 %)	2	8.7 %, a$^{20^\circ C}$	EDB	0.504 ± 0.044 (> 0.90)

671

672 **FIGURES**

673 Figure 1: (a) Predictions of the change in growth factor with RH and the retrieved value of κ if measure-
674 ments were made at different RHs for (a) malonic acid, (b) levoglucosan, and (c) adipic acid from UNIFAC
675 (E-AIM) (blue), UNIFAC with Peng parameters (E-AIM) (green), ADDEM (red) and AIOMFAC (black).
676

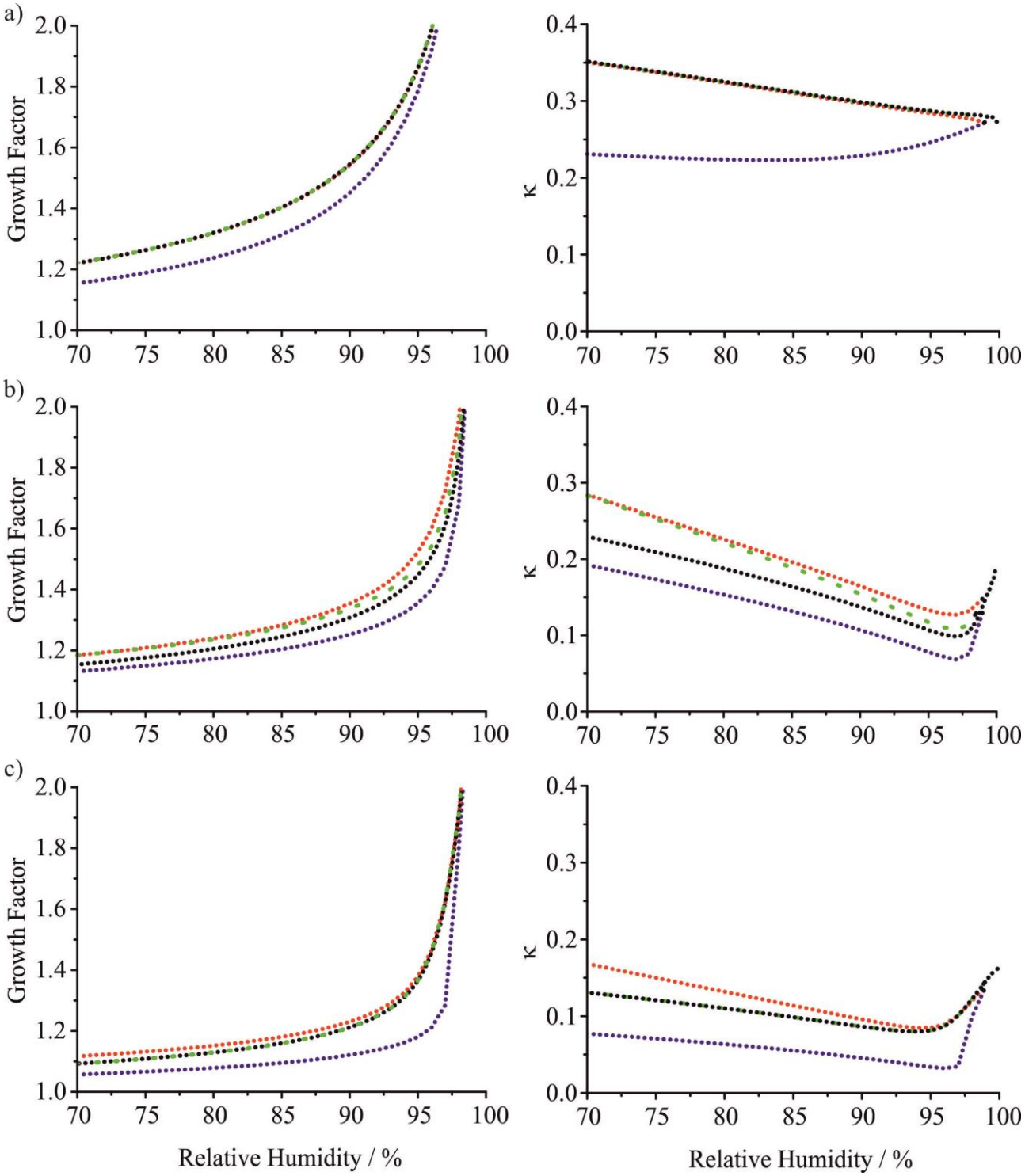

677
678

679 Figure 2: Correlated change in (a) RH, (b) particle radius, and (c) particle RI with time for an aqueous

680 sucrose droplet with dry radius 4145 ± 11 nm held in AOT.

681

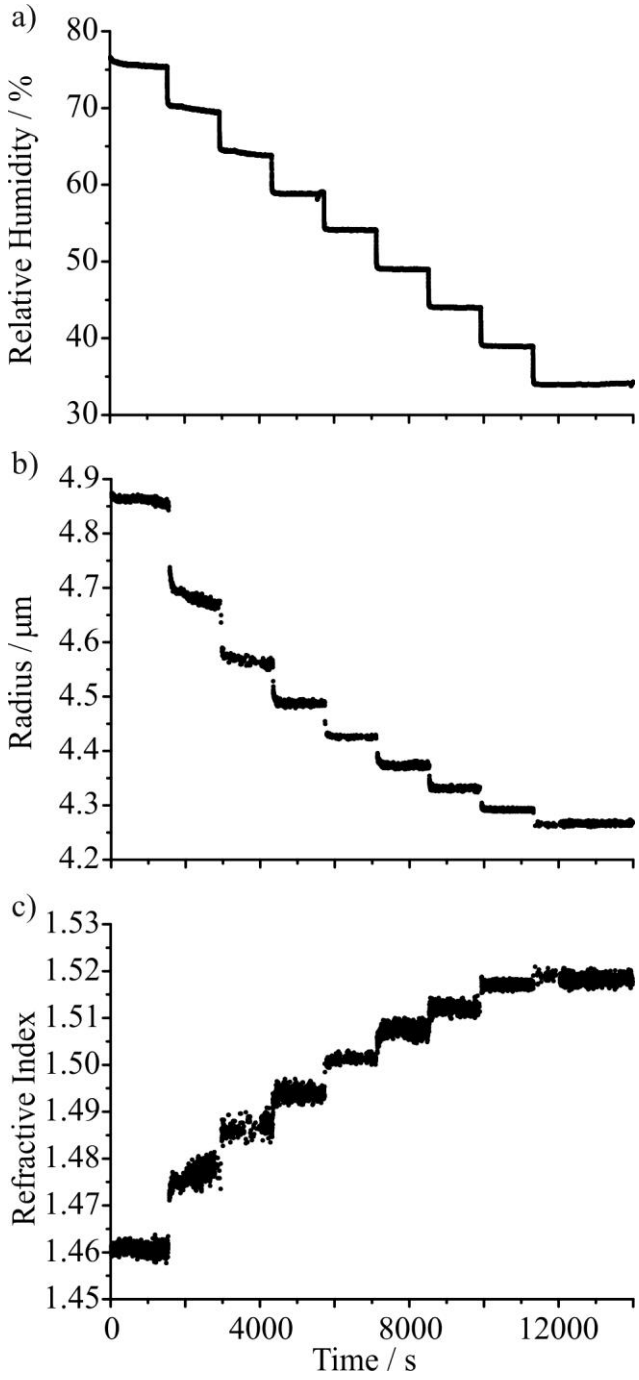

682

683

Figure 3: Refractive index values measured using a refractometer plotted against mfs, with quadratic fits applied to the experimental data. Extrapolation to mfs of one yields refractive index values for pure galactose (black), ascorbic acid (green), sorbitol (purple), xylose (red), and citric acid (orange) of 1.5515 ± 0.0187, 1.5863 ± 0.0320, 1.5260 ± 0.0024, 1.5197 ± 0.0024, and 1.4876 ± 0.0013 respectively. The shaded regions represent the standard error in the quadratic fits. Knowledge of the pure component refractive index is vital for determination of the aerosol droplet dry size, and in turn the *GF*.

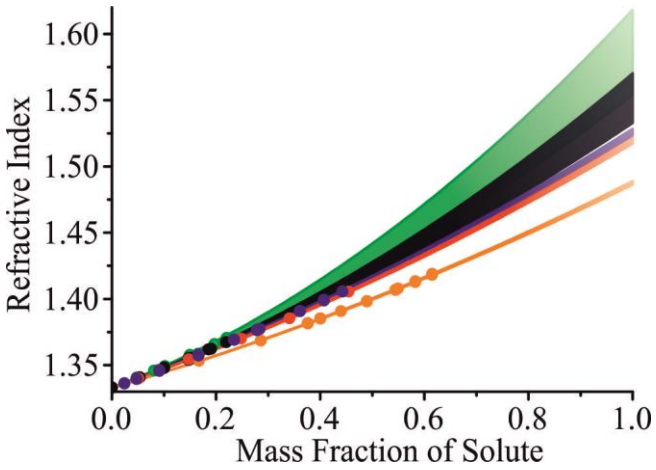

Figure 4: (a) An example of the comparative kinetic measurement showing consecutive evaporation of pure water (grey) and tartaric acid (black) solution droplets into an RH of ~0.95. (b) The growth curve derived from the mass flux data averaged over all tartaric acid droplets and resolved at each size point, with an average taken every 200 points (equivalent to 2 s of mass flux). Uncertainty in *GF* lies within the bounds of the data points. Inset shows the growth factor as a function of measured mass flux, used to calculate the droplet water activity.

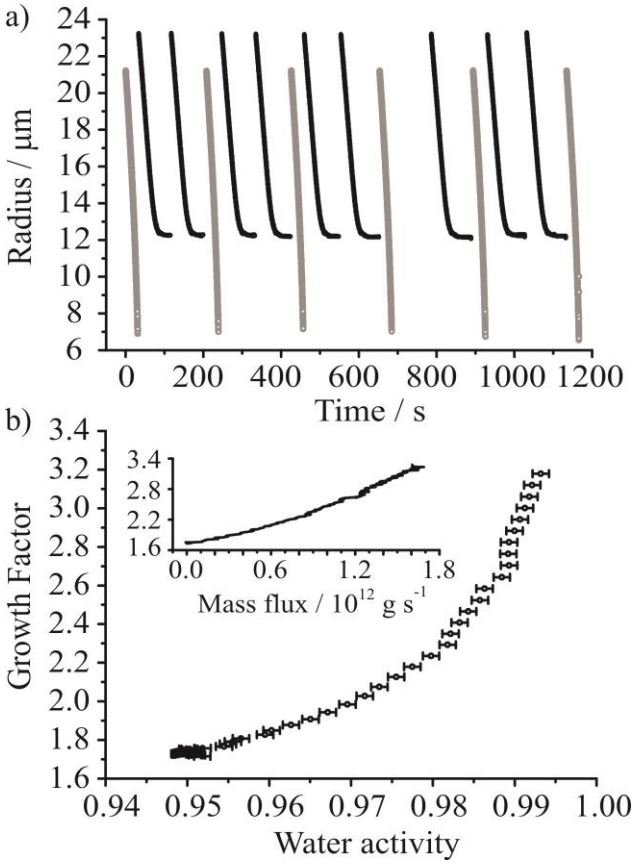

Figure 5: (a) Simulated evaporation profiles for droplets containing a fixed amount of a dissolved species with varying values of κ, illustrating the sensitivity of the EDB evaporation method for measuring hygroscopic growth. The inset shows the long time equilibrium behaviour. We present simulated data in order to show the effect of changing κ while keeping all other variables the same, for instance how the density changes with radius. (b) As an example of the experimental data, measurement data sets of the evaporation kinetics from aqueous droplets of oxalic acid at 93.8 % RH (blue) and tartaric acid at 94.8 % RH (black). Both compounds had an initial concentration of 50.2 g L^{-1}.

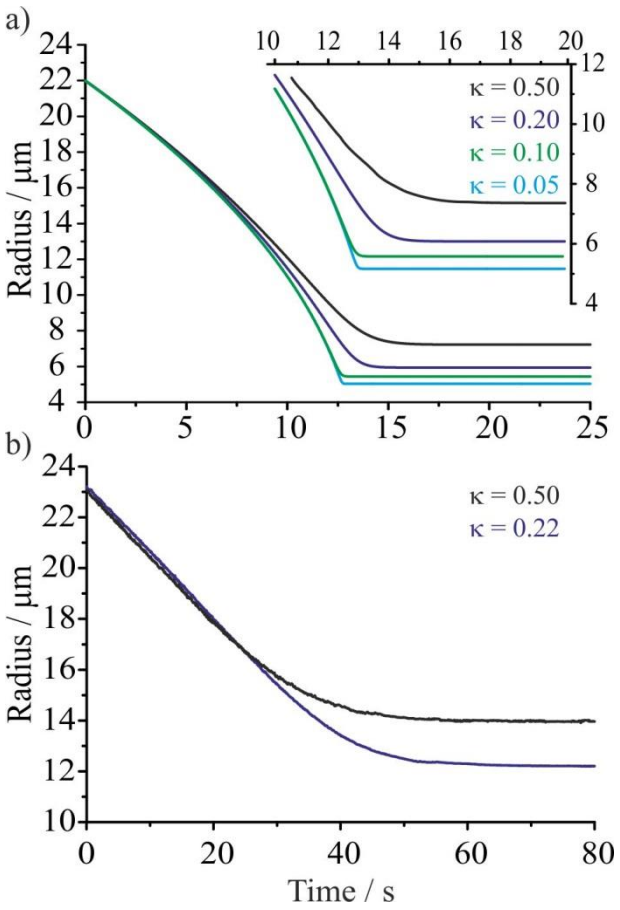

Figure 6: A comparison between experimental data obtained from AOT measurements (at lower water activity) and EDB measurements (at higher water activity) for five representative compounds: malonic acid, tartaric acid, galactose, sorbitol and adipic acid (dark to light grey points, top to bottom). The lines associated with galactose and sorbitol represent linear fits using data from both techniques. The break in the water activity axis and the change in scale should be noted.

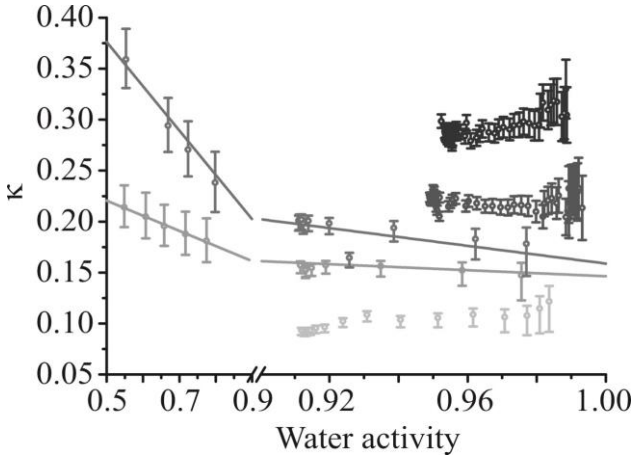

721 Figure 7: Experimentally determined κ values from AOT (red) and EDB (blue) measurements as a function

722 of O/C and data from the literature survey described in the text (grey).

723

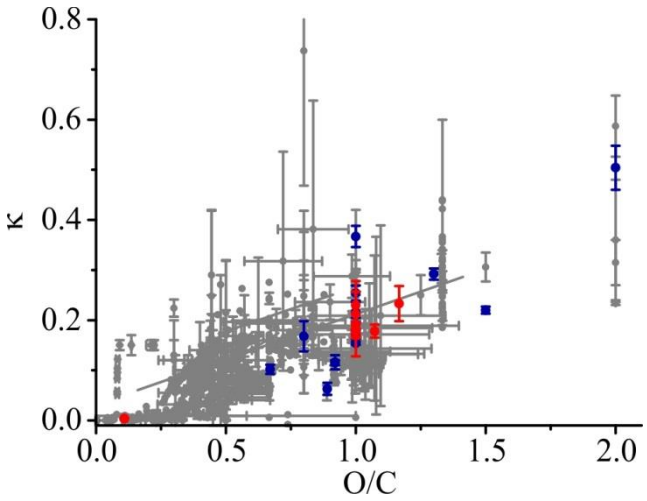

724

725

726 Figure 8: Review of literature data showing the relationship between O/C and κ, with the three
727 panels highlighting data recorded (a) at subsaturated RH (red) and supersaturated RH (grey), (b) in
728 field studies (red) and in laboratory studies (grey) and (c) where the O/C of the aerosol was well-
729 defined (red), and where O/C was inferred from AMS measurements (grey).
730

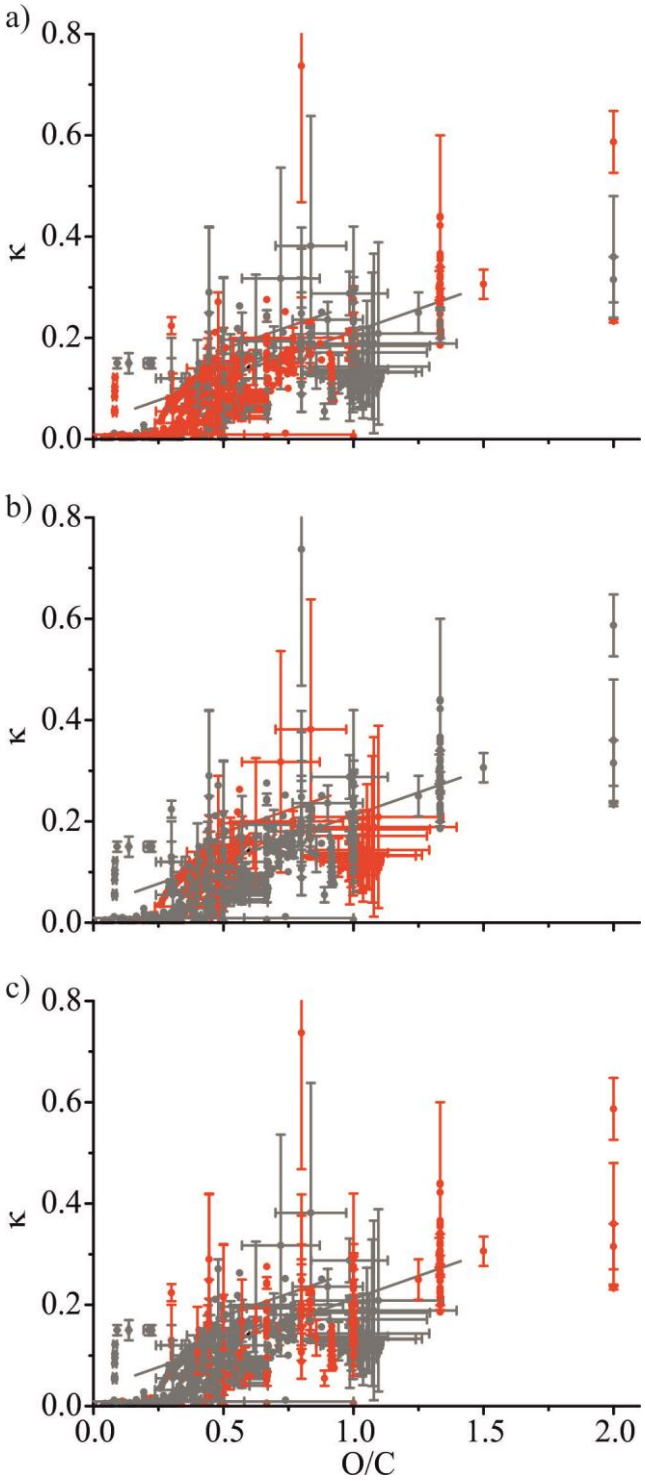

731
732

733 Figure 9: All new experimental and literature data binned by O/C in intervals of 0.1 in terms of (a) κ and (b)
734 predicted critical supersaturation (for a 100 nm diameter aerosol particle). The error bars represent the
735 standard deviation of the average reported κ value, and do not include any experimentally associated error
736 with each of the measurements reported in the literature. A linear fit to this binned data for κ and O/C has
737 been included (grey shaded area), along with previously proposed linear relationships by Chang et al.[53]
738 (green shaded area) and Duplissy et al.[7] (red lines).

739

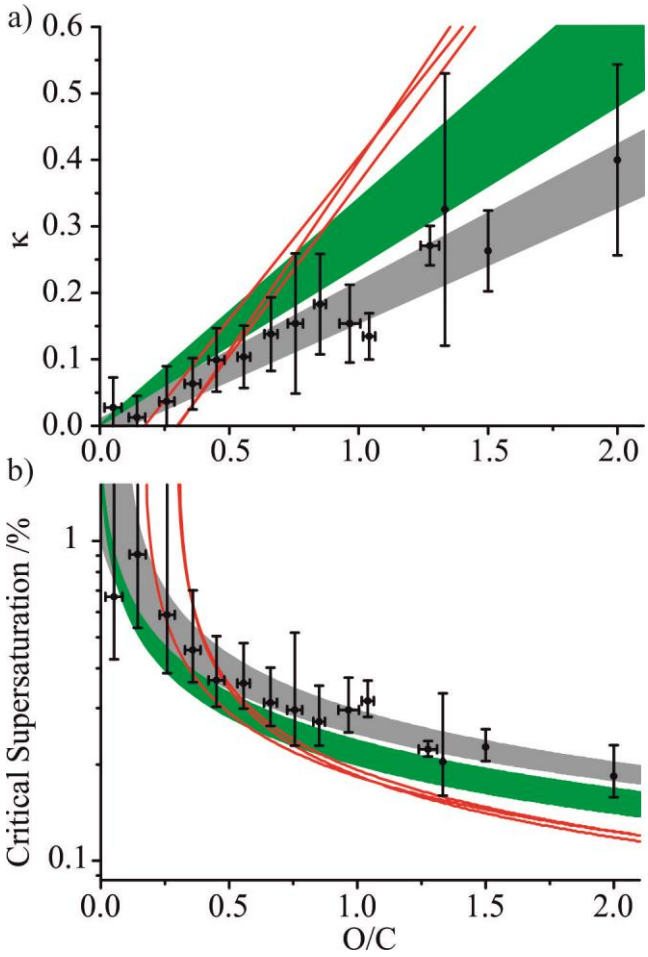

740

741

742 Figure 10: Variation in predicted critical supersaturations with O/C from the linear fit (and uncertainties) to κ
743 for the experimental and literature data. The shaded areas represent aerosol droplets of different dry
744 diameter: 50 nm, 100 nm, and 150 nm, from top to bottom.

745

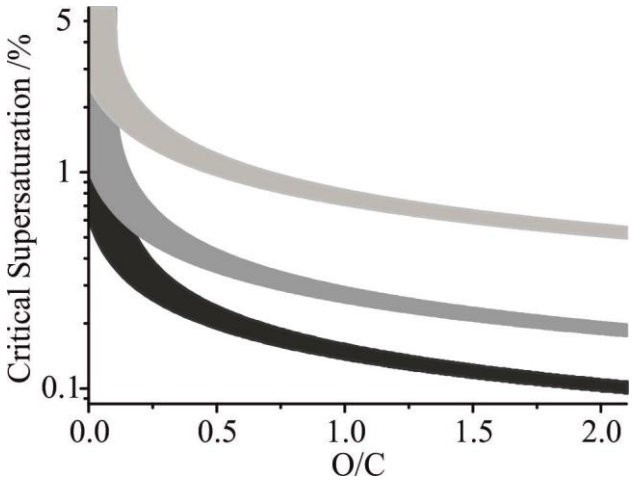

746